UGS-1m: Fine-grained urban green space mapping of ~~34~~ 31 major cities in China based on the deep learning framework

Qian Shi[1,2], Mengxi Liu[1,2,*], Andrea Marinoni[3,4], and Xiaoping Liu[1,2]

[1]School of Geography and Planning, Sun Yat-sen University, Guangzhou 510275, China
[2]Guangdong Key Laboratory for Urbanization and Geo-simulation, Guangzhou 510275, China
[3]Dept. of Physics and Technology, UiT the Arctic University of Norway, 9019 Tromsø, Norway
[4]Dept. of Engineering, University of Cambridge, Cambridge CB2 1PZ, UK

Correspondence: Mengxi Liu (liumx23@mail2.sysu.edu.cn)

Abstract. Urban green space (UGS) is an important component in the urban ecosystem and has great significance to the urban ecological environment. Although the development of remote sensing platforms and deep learning technologies have provided opportunities for UGS mapping from high-resolution images (HRIs), challenges still exist in its large-scale and fine-grained application, due to insufficient annotated datasets and specially designed methods for UGS. Moreover, the domain
5   shift between images from different regions is also a problem that must be solved. To address these issues, a general deep learning (DL) framework is proposed for UGS mapping in the large scale, and the fine-grained UGS maps of ~~34 major cities /areas in China~~ 31 major cities in China Mainland are generated (UGS-1m). The DL framework consists of a generator and a discriminator. The generator is a fully convolutional network designed for UGS extraction (UGSNet), which integrates attention mechanisms to improve the discrimination to UGS, and employs a point rending strategy for edge recovery. The discriminator
10   is a fully connected network aiming to deal with the domain shift between images. To support the model training, an urban green space dataset (UGSet) with a total number of 4,454 samples of size 512×512 is provided. The main steps to obtain UGS-1m can be summarized as follows: a) Firstly, the UGSNet will be pre-trained on the UGSet in order to get a good starting training point for the generator; b) After pre-training on the UGSet, the discriminator is responsible to adapt the pre-trained UGSNet to different cities/areas through adversarial training; c) Finally, the UGS results of the ~~34 major cities /areas~~ 31 major
15   cities in China (UGS-1m) are obtained using 2,343 Google Earth images with a data frame of 7'30" in longitude and 5'00" in latitude, and a spatial resolution of nearly 1.1 meters. Evaluating the performance of the proposed framework on samples from five sample cities shows the validity of the UGS-1m products, with an ~~avgrage~~ average overall accuracy (OA) of 87.56% and an F1 score of 74.86%. Comparative experiments on UGSet with the existing state-of-the-art (SOTA) DL models proves the effectiveness of UGSNet as the generator, with the highest F1 of 77.30%. Furthermore, ablation study on the discriminator
20   fully reveal the necessity and effectiveness of introducing discriminator into adversarial learning. Finally, the comparisons with existing products further shows the feasibility of the UGS-1m and the effectiveness and great potential of the proposed DL framework. The UGS-1m can be downloaded from https://doi.org/10.5281/zenodo.6155516 (Shi et al., 2022).

1 Introduction

Urban green space (UGS), one of the most important components of the urban ecosystem, refers to the vegetation entity in the urban area (Kuang and Dou, 2020), such as parks and green buffers. It plays a very important role in the urban ecological environment (Kong et al., 2014; Zhang et al., 2015), public health (Fuller et al., 2007) and social economy (De Ridder et al., 2004). ~~However, in the context of rapid urbanization,~~ In recent years, driven by the policies of the Sustainable Development, how to provide equality UGS resources for urban residents has increasingly become the goal of local governments and institutions (Chen et al., 2022b). In the process of policy development and funding to achieve more equal access to green space, it is necessary to master the UGS distributionof resources (Zhou and Wang, 2011; Huang et al., 2018; Zhao et al., 2010). Though statistical data, such as Statistics Yearbook, can provide approximate area of UGS for a certain region or city, it is difficult to obtain exact distribution of the UGS. In addition, for some districts, the UGS ~~is now facing drastic changes in terms of sustainability, integrity and diversity. Indeed, some UGS changes might have a negative impact on the fragile urban ecosystem and cause a series of problems on the urban environment and welfare. In technical literature, several works have enthusiastically discussed the interaction mechanism between UGS and urban environment, in which relevant UGS data is indispensable (see for instance Zhou and Wang, 2011; Huang et al., 2018; Zhao et al., 2010).~~ distribution information is often unavailable or unreliable. These phenomena have greatly hindered the effective formulation of relative policies, and the efficient allocation . Thus, to provide the reliable basic geographic data for in-depth UGS research, fast and accurate mapping of UGS is crucial and necessary.

With the development and application of remote sensing technology, diversified remote sensing data ~~are increasingly used~~ have provided more objective approaches to obtain UGS coverage. In this respect, multispectral remote sensing images are widely used. Sun et al. (2011) extracted UGS in China's 117 metropolises from MODIS data over the last three decades through Normalized Difference Vegetation Index (NDVI), to study its impacts on urbanization. Huang et al. (2017) obtained urban green coverage of 28 megacities from Landsat images between 2005 and 2015 to assess the change of health benefits by urban green spaces. Recently, taking advantage of cloud computing, many excellent land cover products based on Landsat and Sentinel-1&2 images have been proposed, including GlobeLand30 (Jun et al., 2014), GLC_FCS30 (Zhang et al., 2021) , FROM_GLC10 (Gong et al., 2013), Esri 2020 LC (Helber et al., 2019). These products have provided valuable world-wide maps of land coverage, so that researchers can easily extract relevant information and conduct in-depth research on specific UGS properties, such as impervious surface, UGS coverage, etc. Although multispectral images have provided powerful data support for large-scale and long-term UGS monitoring, it is often difficult to obtain UGS information of small scale due to the limitation of spatial resolution of multispectral images. In other words, some small-scale UGSs (such as UGS attached to buildings and roads) are difficult to be identified in multispectral images, although they are of great significance to urban ecosystem. Therefore, images with higher spatial resolution are required to address the large difference in intra-class scale of urban green space.

To get finer-grained extraction of UGS, remote sensing imagery with richer spatial information are more and more employed in UGS extraction, such as Rapid-Eye, ALOS and SPOT images (Mathieu et al., 2007; Zhang et al., 2015; Zhou et al., 2018).

In these studies, machine learning methods, including SVM (Yang et al., 2014) and random forest (Huang et al., 2017), are often employed to obtain UGS coverage. However, hand-craft features are required for classification in these methods, which are time- and labor-consuming, and not objective enough.

60   Deep learning (DL) based methods can hence be used to address these issues (Deng and Yu, 2014). In fact, DL schemes can extract multi-level features automatically, so that they are becoming the mainstream solution in many fields, including computer vision, natural language processing, medical image recognition, etc (Zhang et al., 2018; Devlin et al., 2018; Litjens et al., 2017). Among DL algorithms, the full convolution networks (FCNs), represented by UNet (Ronneberger et al., 2015), SegNet (Badrinarayanan et al., 2017) and Deeplab v3+ (Chen et al., 2018a), have been widely introduced into remote sensing

65   interpretation tasks, such as building footprint extraction (Liu et al., 2019a), change detection (Liu et al., 2021), as well as UGS mapping (Liu et al., 2019b). For instance, Xu et al. (2020) improved the U-Net model by adding batch normalization (BN) and dropout layer to solve the over-fitting problem, and monitored UGS areas in Beijing. Liu et al. (2019b) employed DeepLab v3+ to automatically obtain green space distribution from ~~GF-2~~ GaoFen-2 (GF2) satellite imagery. With the help of convolutional operators with different receptive fields for multi-scale feature extraction and fully convolutional layers to

70   recover spatial information, the FCN methods can achieve accurate pixel-level results in an end-to-end manner (Daudt et al., 2018).

In the context of rapid changes in the global ecological environment, large-scale and high-resolution automatic extraction of UGS is becoming more and more important (Cao and Huang, 2021; Wu et al., 2021). Although the existing methods have achieved good results in UGS extraction based on deep learning, there are still open problems to be solved. Firstly, significant

75   intra-class differences and inter-class similarities of UGS have jeopardized the classic strategies for recognition of UGS. The appearance and scale of UGS vary significantly due to the wide variety involved. For example, while the green buffers inside roads are measured in meters, a public park could be measured in kilometers. Moreover, the substantial similarity between farmland and UGS also leads to severe misclassification, while farmland does not belong to UGS. Therefore, guaranteeing that the model can extract effective relevant features is crucial to accurately obtain UGS coverage.

80   Secondly, the development of UGS extraction methods based on deep learning framework is greatly limited by the lack of datasets, while accurate and reliable results by deep learning models heavily rely on sufficient training samples. The last few decades have witnessed the flourishing of many large datasets to be used for deep learning architectures, such as ImageNet (Krizhevsky et al., 2012), PASCAL VOC (Everingham et al., 2015), SYSU-CD (Shi et al., 2021). Nevertheless, due to tremendous time and labor required, there are few publicly available datasets with fine-grained UGS information. This condi-

85   tion reduces the efficiency of researchers, and hinders the fair comparison between UGS extraction methods, not to mention providing reliable basic data for large-scale UGS mapping.

Last but not least, the large-scale fine-grained UGS mapping is also limited by the difference of data distribution. Affected by external factors (e.g., illumination, angle and distortion), remote sensing images collected in different regions and time are difficult to keep consistent data distribution. Therefore, the model trained on a certain dataset fail to be well applied to images

90   of another region. In order to overcome the data shift between difference data, domain adaptation should be adopted to improve the generalization of the model.

In ~~view of the aforementioned problems~~order to provide fine-grained maps and explore a mapping diagram for diversified UGS research and analysis, we develop a deep learning framework for large-scale and high-precision UGS extraction, leading to a collection of 1-meter UGS products of ~~34 major cities /areas~~ 31 major cities in China (UGS-1m). As shown in Figure 1, we firstly construct a high-resolution urban green space dataset (UGSet), which contains 4,454 samples of size 512×512, to support training and verification of UGS extraction model. Then we build a deep learning model for UGS mapping, which consists of a generator and a discriminator. The generator is a fully convolutional network for UGS extraction, also referred as UGSNet, which integrates an enhanced Coordinate attention (ECA) module to capture more effective feature representations, and a point head module to get fine-grained UGS results. The discriminator is a fully connected network that aims to adapt the UGSet-pretrained UGSNet to large-scale UGS mapping through adversarial training (Tsai et al., 2018). Finally, the UGS results of the ~~34 major cities /areas~~ 31 major cities in China, namely UGS-1m, are obtained after post-processing, including mosaic and mask.

The contributions of this paper can be summarized as follows:

(1) ~~a general deep learning framework for large-scale and high-resolution UGS mapping, and generating UGS maps of 34 major cities /areas~~ the UGS maps of 31 major cities in China with a spatial resolution of 1 meter (UGS-1m) ~~, is proposed~~is generated based on a proposed deep learning framework, which can provide fine-grained UGS distribution for relevant studies;

(2) a fully convolutional network for fine-grained UGS mapping (UGSNet) is introduced. This architecture integrates an enhanced Coordinate attention (ECA) module and a point head module to address the intra-class differences and inter-class similarities in UGS;

(3) a large benchmark dataset, Urban Green Space dataset (UGSet), is provided to support and foster the UGS research based on the deep learning framework;

The reminder of this paper is arranged as follows. Sect. 2 introduces the study area and data. Sect. 3 illustrates the deep learning framework for UGS mapping. Sect. 4 assesses and demonstrates the UGS results. Then discussions will be conducted in Sect. 5. The access to the code and data is provided in Sect. 6. Finally, conclusions will be made in Sect. 7.

2 Study area and data

2.1 Study area

In recent years, in order to satisfy the concept of ecological civilization and sustainable development, scientific urban green space planning and management have been paid more and more attention in China (General Office of the State Council, PRC, 2021). Therefore, how to improve the rationality of UGS classification system and layout distribution to build a healthy and livable city has been the focus of government and scholars in recent years(Ministry of Housing and Urban-Rural Development, PRC, 2019; Chen et al., 2022a). To this end, this paper selects ~~34 major cities /areas~~ 31 major cities in China as study area,
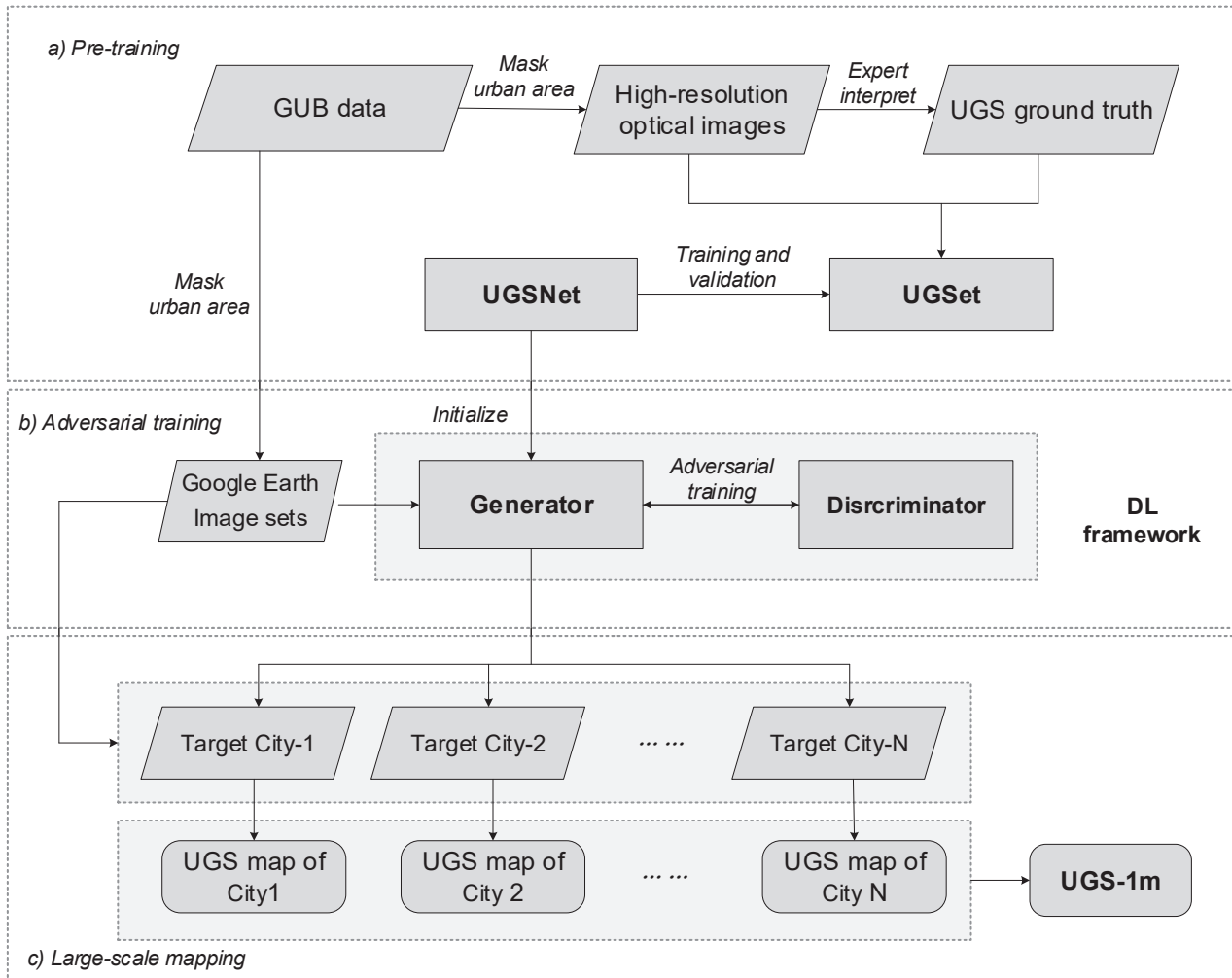
Figure 1. Diagram of the deep learning framework to generate UGS-1m. a) Pre-train the proposed UGSNet on the UGSet dataset; b) Optimize the generator (initialized by UGSNet) to different target cities with a discriminator through adversarial training; c) Apply each optimized generator to corresponding target city for large-scale mapping.

aiming to construct a comprehensive UGS dataset for deep learning model training under the official classification system, and generate high-resolution green space mapping for each city/area.

125   As Figure 2 shows, the study area includes ~~two special administrative regions (Hong Kong and Macau),~~ four municipalities (Beijing, Shanghai, Tianjin, and Chongqing), capitals of five autonomous regions (Huhuhot, Nanning, Lasa, Yinchuan and Urumqi), as well as captials of ~~23 provinces~~ 22 provinces in Chinese mainland (Harbin, Changchun, Shenyang, Shijiazhuang, Lanzhou, Xining, Xi'an, Zhengzhou, Jinan, Changsha, Wuhan, Nanjing, Chengdu, Guiyang, Kunming, Hangzhou, Nanchang, Guangzhou, Fuzhou, ~~Taipei,~~ Haikou).
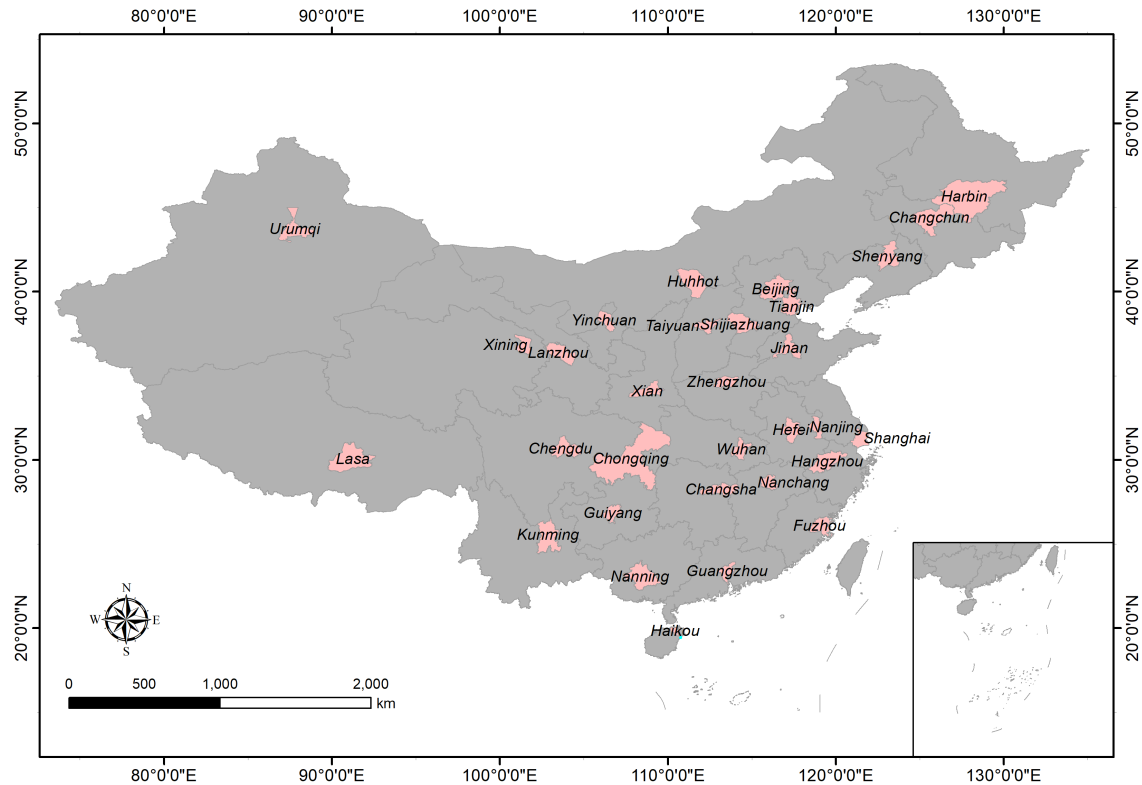
Figure 2. ~~The 34~~ Distribution of the 31 major cities ~~/areas~~ in China.

2.2 Datasets

2.2.1 UGSet

Urban green space can be divided into five categories, including park, green buffer, square green space, attached green space and other green space (Chen et al., 2018b), as described in Table 1. Different types of UGS vary not only on their functions, but also on shape and scale: these properties become more apparent in high-resolution images. For instance, park and green buffer are often occurring in a relatively large volume, while attached green space and square green space are mainly scattered in urban areas in smaller form. In other words, urban green space is not only diverse, but also has large inter- and intra-class scale differences. Therefore, a dataset that contains UGS samples of different types and scales is an important guarantee for the model to learn and identify UGS accurately.

In order to provide an extensive sample database for wide-range UGS mapping, as well as a benchmark for comparisons among deep learning algorithms, we constructed a largescale high-resolution urban green space dataset (UGSet), which con-

Table 1. UGS types and descriptions.

Type	Description
Park	Green space open to the public for all kinds of outdoor activities
Green buffer	Green space to isolate facilities like sewage treatment plants, garbage treatment plants, high-voltage lines, etc, or water bodies such as rivers, lakes and seas
Square green space	Green space in open scape area with leisure and entertainment functions, mainly is shrubs and grassland
Attached green space	Green space attached to residential, transportation, industrial, or commercial land
Other green space	Green space on undefined land

tains 4,544 images of size 512×512 with a spatial resolution of nearly 1 meter. These images ~~acquired by Gaofen-2~~ are collected from 142 images in Guangdong Province, China, as shown in Figure 3~~.~~, through the Gaofen-2 (GF2) satellite. The GF2 satellite is the first civilian optical remote sensing satellite developed by China with a spatial resolution of about 1 meter, which is equipped with two high-resolution 1-meter panchromatic and 4-meter multispectral cameras. With the aim to filter out green

145 space in non-urban areas, the global urban boundaries (GUB) data (Li et al., 2020) of 2018 is used to mask the urban areas of each original image. All types of UGS in the images are carefully annotated through expert visual interpretation, before they are cropped into 512×512 patches. As can be seen from Figure 4, the category of non-UGS and UGS in the ground truth are represented by 0 and 255, respectively. According to the ratio of 5:2:3, the UGSet is randomly divided into the training set, verification set and test set.

150 **2.2.2   Global urban boundaries (GUB)**

The global urban boundaries (GUB) data (Li et al., 2020) that delineate the boundary of global urban area in seven years (i.e. 1990, 1995, 2000, 2005, 2010, 2015, and 2018) is obtained by processing the 30 m global artificial impervious area (GAIA) data (Gong et al., 2020). It is worth noting that GAIA is the only annual map of impervious surface areas from 1985 to 2018 with a resolution of 30 m. In this study, the GUB data in 2018 are adopted to mask the urban area. Specifically, in order to

155 obtain accurate UGS samples, the GUB data are used to filter out non-relevant green space samples from non-urban areas. The GUB data are also applied to the UGS results from the model for post processing, so to get final UGS map of each city/area.

2.2.3   Google Earth Imagery

Google Earth is a free software which enables users to view high-resolution satellite images around the world. Therefore, in order to obtain fine-grained UGS maps in the study area, a total number of 2,343 Google Earth images covering ~~34 major cities~~

160 ~~/areas~~ 31 major cities in China are downloaded, each with a data frame of 7'30" in longitude and 5'00" in latitude, and a spatial
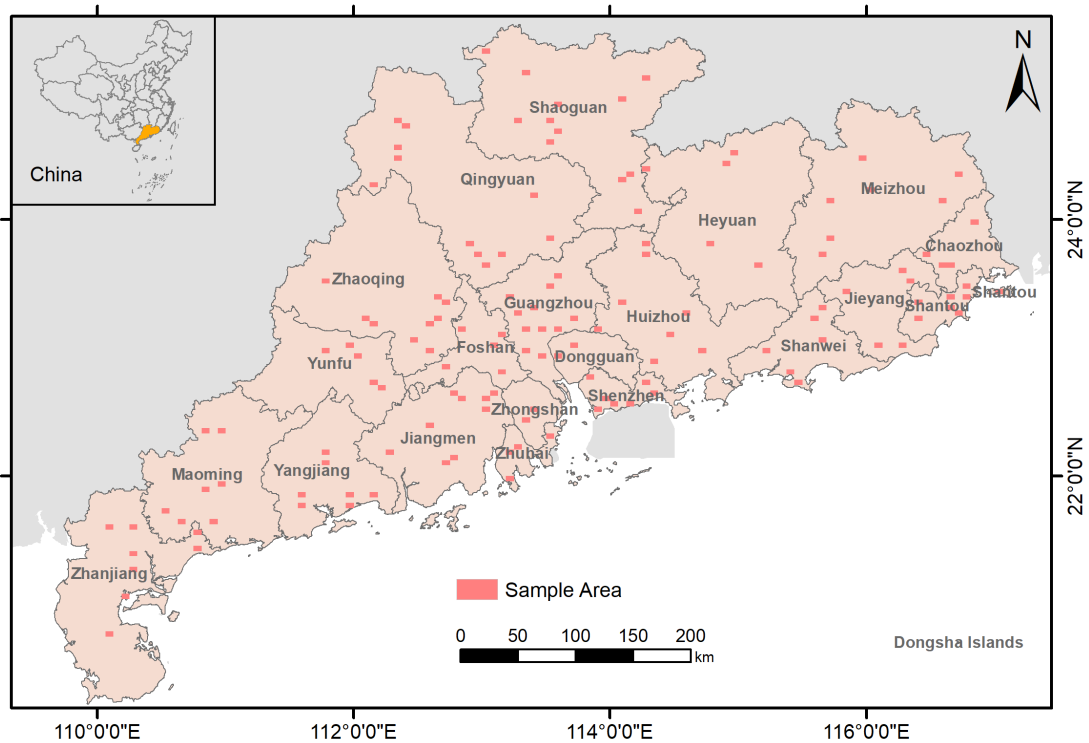
Figure 3. The 142 Sample areas in UGSet collected from Guangdong Province. Each with a data frame of 3'45 "in longitude and 2'30" in latitude.

resolution of nearly 1.1 meters. All images selected are clear and cloud-free to avoid missed detection. Limited by the GPU memory, these images are all cropped into the size of 512×512 for prediction.

3 Methods

In order to realize large-scale fine-grained UGS mapping, a general model framework is essential, in addition to a sufficiently large dataset. Therefore, we propose a deep learning framework for UGS mapping: its functional flowchart is shown in Figure 5. Inspired by adversarial domain adaptation frameworks (Tsai et al., 2018), the proposed framework includes a generator and a discriminator. In particular, a fully convolutional neural network, namely UGSNet, is designed as the generator: this structure is utilized to learn and extract fine-grained UGS information. On the other hand, a simple fully connected network is employed as the discriminator to help model domain adaptation and achieve large-scale UGS mapping.

The following Sect. 3.1 and Sect. 3.2 will introduce the structure of UGSNet and discriminator, respectively. The optimization process of the deep learning framework will be described in Sect. 3.3, which can be divided into two parts: pre-training and adversarial training. Parameter settings and accuracy evaluation will be covered in Sect. 3.4 and Sect. 3.5.

Image

Label

Image

Label

(a)   (b)   (c)   (d)   (e)
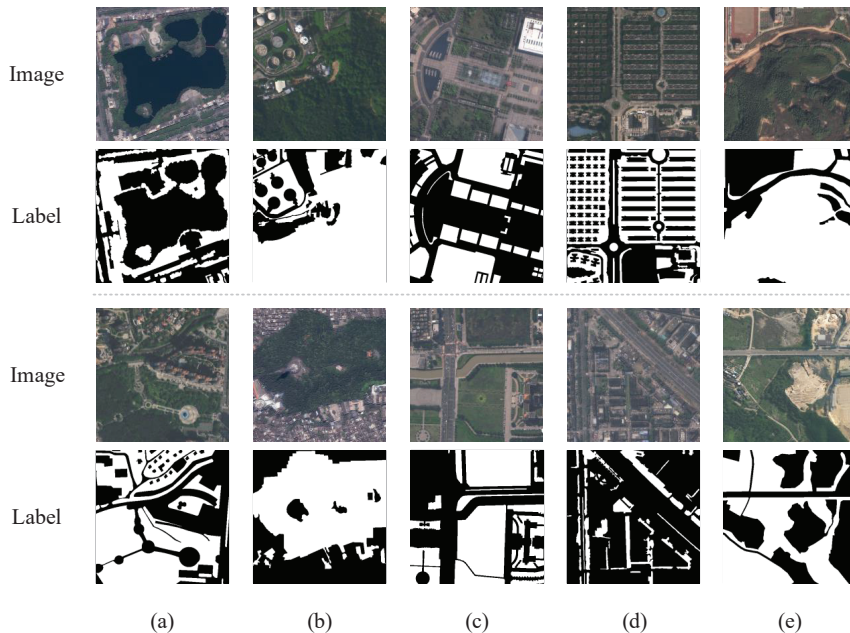
Figure 4. Example of ~~different types of UGS~~ the "Image-Label" samples in UGSet (Images were retrieved from ~~GF-2~~ Gaofen-2 2019). The first and third rows denote images of the samples, while the second and forth rows provide corresponding labels for these images. Each column denotes different UGS types of the samples, including (a) Park; (b) Green buffer; (c) Square green space; (d) Attached green space; (e) Other green space.

3.1 UGSNet

~~As shown in Figure 6,~~ The UGSNet contains two parts: a backbone to extract multi-scale features and generate coarse results, and a point head module to obtain fine-grained results.

~~Architecture of the proposed UGSNet (The image was retrieved from GF-2 2019).~~

3.1.1 Backbone

The ~~backbone of the UGSNet first~~ structure and elements of the backbone is shown in Figure 6, which adopts the efficient ResNet-50 as feature extractor to capture multi-scale features from the images. This segment contains five stages: the first stage consists of a 7×7 convolutional layer, a batch normalization layer (Ioffe and Szegedy, 2015), a Rectified Linear Unit (ReLU) function (Glorot et al., 2011) and a max-pooling layer with a stride of 2; then, four residual blocks are utilized to capture deep features of four different levels. The four residual blocks are connected by four enhanced Coordinate attention (ECA) modules to enhance feature representations.
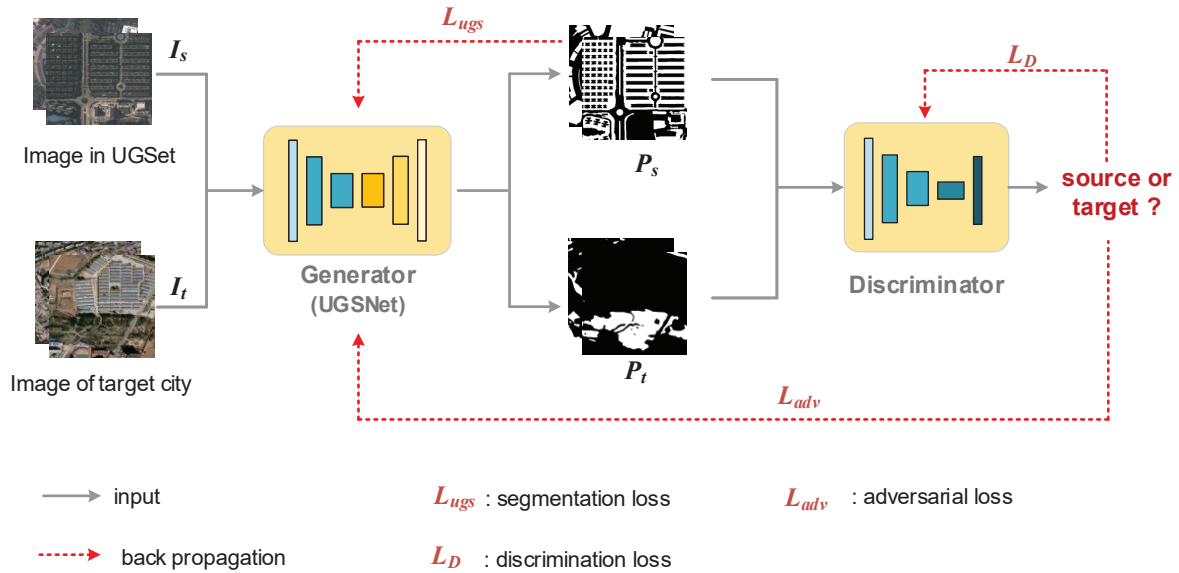
Figure 5. Flowchart of the proposed deep learning framework for UGS mapping (The "Image in UGSet" were retrieved from ~~GF-2~~ Gaofen-2 2019, ~~whiel~~ while the "Image of target city" © Google Earth 2020). The red dashed lines denote the loss of back propagation for model optimization. The L_ugs, L_D, and L_adv represent the segmentation loss, the discrimination loss, and the adversarial loss, as described in Sect. 3.3.

Previous researches have proved that attention mechanism can bring gain effects to deep neural networks (Vaswani et al., 2017; Woo et al., 2018). Recently, a novel "coordinate attention" (CA) (Hou et al., 2021) was proposed, which improved the weakness of traditional attention mechanisms in obtaining long-range dependence by embedding location information efficiently. Specifically, in order to capture the spatial coordinate information in the feature maps, the CA uses two 1-Dimensinal (1D) global pooling layers to encode input features along the vertical and horizontal directions, respectively, into two direction-aware feature maps. However, this approach ignores the synergistic effect of features in two spatial directions. Therefore, we propose the enhanced coordinated attention (ECA). In addition to the original two parallel 1D branches encoding long-distance correlation along the vertical and horizontal direction, respectively, ECA also introduces a 2D feature encoding branch to capture the collaborative interaction of feature maps in the entire coordinate space, so as to obtain a more comprehensive coordinate-aware attention maps for feature enhancement. The structure of the ECA module is shown in Figure ~~7~~6-(c).

Then, four 1×1 convolutional blocks will be applied to the attention-refined features of the four residual blocks to unify their output channels to 96, then they are concatenated together after resizing. Finally, the fused features will be input into two 3×3 convolutional layers to generate a coarse prediction map, which is 1/4 the size of the input image.
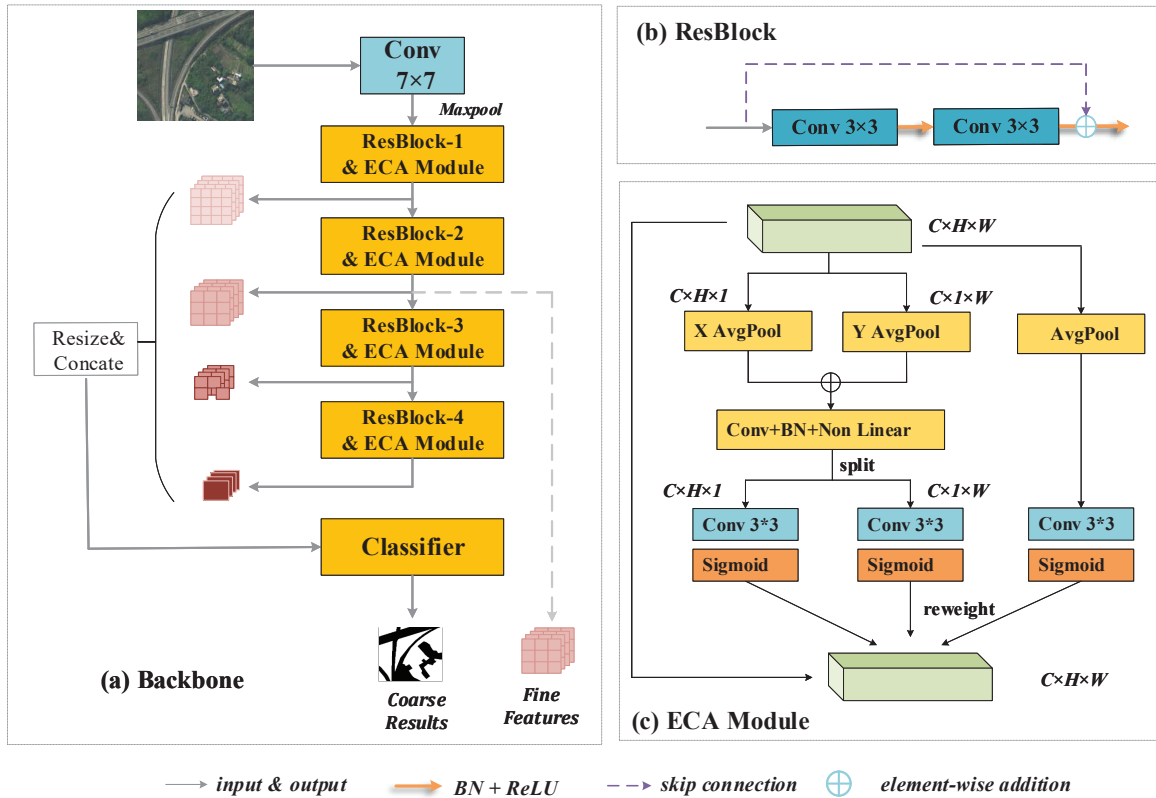
Figure 6. Architecture of the backbone in UGSNet (The image was retrieved from Gaofen-2 2019). (a) Backbone overview. (b) Sketch diagram of the ResBlock. (c) ECA module.

3.1.2 Point Head

Many semantic segmentation networks directly sample high-dimensional features to obtain segmentation results of original image size, which will lead to rough results, especially near the boundary. Therefore, the point head is introduced into UGSNet, which uses the point rendering strategy (Kirillov et al., 2020) to get fine-grained UGS results efficiently. ~~Specifically~~According to Figure 7, given the fine-grained features and the coarse UGS results from the backbone, the specific process in the point head includes the following three steps: 1) firstly, collect N sampling points with lower certainty; 2) then, construct point-wise features of the selected N points based on the coarse UGS results and fine-grained features from the backbone; 3) finally, reclassify the results of the selected N points through a simple multilayer perceptron (MLP). Detailed information of each step will be elaborated in the following.

In the first step, how to adaptively select sample points is the key to improve the segmentation results in an efficient and effective way, so different sampling strategies are adopted in the training and inference process. At the training stage, different
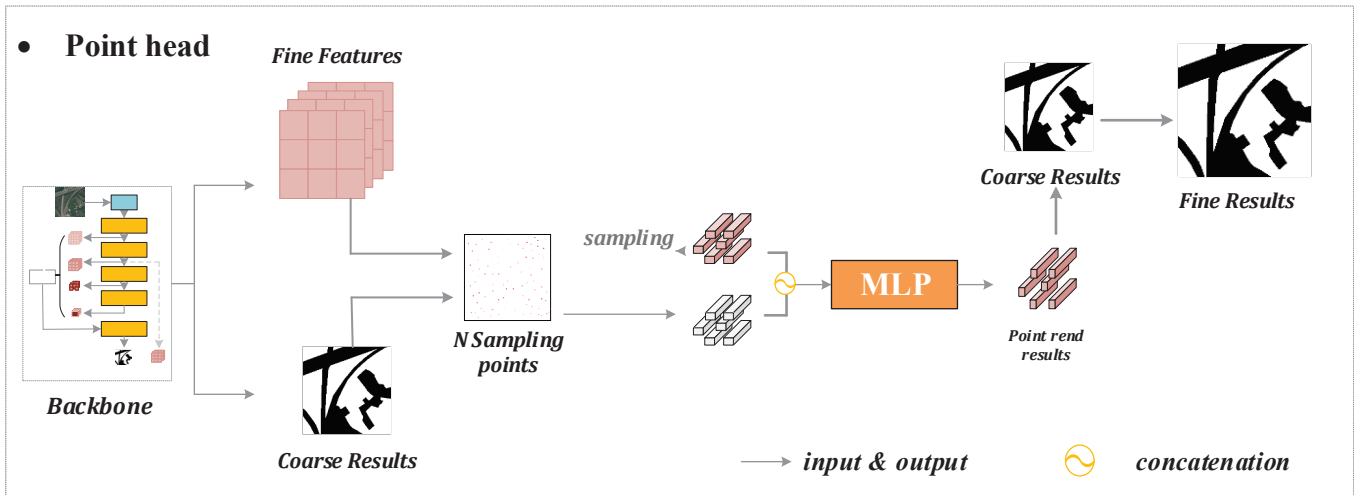
Figure 7. Structure of the ~~enhanced Coordinate attention (ECA) module~~ point head in UGSNet. Given the fine features and the coarse UGS results from the backbone, the point head will firstly collect N sampling points with lowest certainty to construct point-wise features, which will be input into a MLP for classification and help obtain fine UGS results.

points are expected to be taken into account. Therefore, at first $k \times N$ points will be randomly generated from the coarse segmentation results as candidates; then, $\beta \times N$ ($\beta \in [0,1]$) points with highest uncertainty will be selected from the $k \times N$ ones; after that, the other $(1-\beta) \times N$ points will be randomly selected from the remaining candidates to supplement. In the inference process, the N sampling points are directly selected from the candidate points with highest uncertainty to consider more hard points. The second step is to build point-wise features based on the N sampling points obtained in the previous step. The coarse prediction and the selected fine-grained features from the backbone (the output of Res-Block2 in this paper) corresponding to each sampling point will be concatenated to obtain point-wise features, so that the feature can contain both local details and global context. Finally, the point-wise features will input into an MLP, which is a 1×1 convolutional layer actually, to obtain new classification results for each point. In our experiments, N=1024 sampling points will be collected, and the value of k and β are 3 and 0.75, respectively.

3.2 Discriminator

In order to transfer the prior knowledge from UGSet to images from other regions, a discriminator is adopted to obtain a well-adapt UGSNet for each city/area in an unsupervised way. As shown in Figure 8, the discriminator consists of five convolutional layers with a kernel size of 4 and a stride of 2, each connected by a Leaky ReLU layer. The output channels of each convolutional layers are 64, 128, 256, 512, and 1, respectively. Given an input of the softmax prediction map from the generator, $P \in R^{H \times W \times C}$, the discriminator will output a discriminant result of the input, $D(P) \in R^{h \times w \times 1}$. After that, the discriminator will optimize itself according to the discrimination accuracy through the cross-entropy loss in (4).
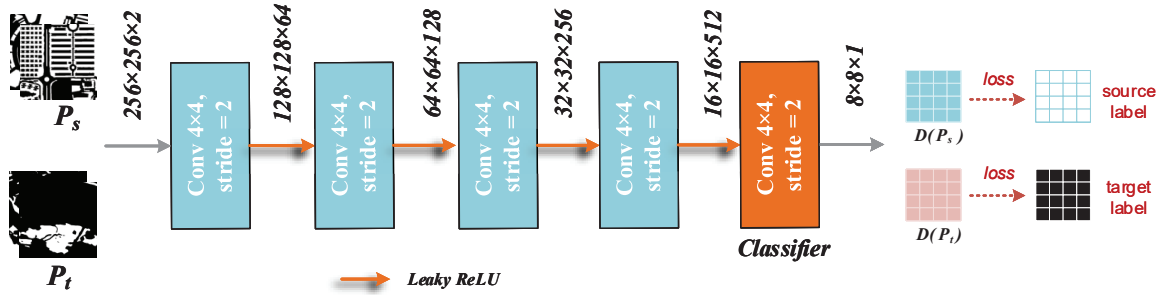
Figure 8. The structure of the discriminator.

3.3 Optimization

The training of the proposed deep learning framework can be divided into two steps: pre-training, and adversarial training. At the beginning, the UGSNet will be fully trained on UGSet to get initial parameters for the generator. After that, the discriminator will be adopted to help generalize the pre-trained UGSNet to target cities/areas through adversarial learning. Detail information of the optimization process are described in the following.

3.3.1 Pre-training

In the pre-training process, the UGSNet will learn characteristics of all kinds of UGS from UGSet. Let us suppose the coarse result output by the backbone is X and the ground truth is Y. Then, the loss between Y and X is calculated by a dice loss, which can be defined as follows:

$$L_{Dice} = 1 - (2|X \cap Y|)/(|X| + |Y|) \tag{1}$$

where $|X \cap Y|$ is the intersection between X and Y, whilst $|X|$ and $|Y|$ denote the number of elements of X and Y, respectively.

The loss of the classification results of the N sampling points in the point head is measured by the cross-entropy loss, which can be defined as

$$L_{CE} = -\sum_{i}^{N}[x_i log y_i + (1 - x_i)log(1 - y_i)] \tag{2}$$

where x_i and y_i represent the results and ground truth of the i-th point among the N sampling ones, respectively.

Finally, the UGSNet is optimized by a hybrid loss, which can be expressed by

$$L_{ugs} = L_{Dice} + L_{CE} \tag{3}$$

3.3.2 Adversarial training

After pre-training, the UGSNet is employed as the generator in the deep learning framework and train with the discriminator to obtain a model that can be used for the UGS extraction of a target city/area. Taking the image I_s and ground truth Y_s in UGSet,

and the image I_t from the target city/area as input, the adversarial training process requires no additional data for supervision, which can be summarized as follows:

(1) Taking the pre-trained UGSNet as the start training point of the generator, the I_s and I_t are forward to the generator G to get their prediction result P_s and P_t, which can be denoted as

$$P_s, P_t = G(I_s), G(I_t) \tag{4}$$

(2) Input P_s and P_t into the discriminator D in turn to distinguish the source of the inputs;

(3) According to the judgement result, the discriminator D will be optimized first, which can be denoted as

$$L_D(P) = -[(1-y)log(D(P)^{(h,w,0)}) + ylog(D(P)^{(h,w,1)})] \tag{5}$$

where y represents the source of the inputs, and $y = 0$ denotes an input P of P_t, and $y = 1$ denotes an input of P_s.

(4) Then, an adversarial loss L_adv is calculated to help promote the generator G to produce more similar results to confuse the discriminator. The L_adv is actually the loss when the discriminator D misclassifies the source of P_t as I_s, which can be expressed as

$$L_{adv} = -log(D(P_t)^{(h,w,1)}) \tag{6}$$

(5) Finally, the generator will be optimized through the following objective function:

$$L_G = L_{ugs} + L_{adv} \tag{7}$$

3.4 Parameter settings

During the pre-training process, the training set of the UGSet is used for parameter optimization, to which random crop, flip and rotation are employed for data augmentation to avoid overfitting, while the verification set was used to monitor the training direction and save the model in time. Five common semantic segmentation models are selected for comparison to prove the validity of UGSNet, including UNet (Ronneberger et al. 2015), SegNet (Badrinarayanan et al. 2017), UperNet (Xiao et al. 2018), BiSeNet (Yu et al. 2018) and PSPNet (Zhao et al. 2017). In addition, ablation study is also conducted to further verify the effectiveness of the ECA modules and the point head. All models are fully trained for 200 epochs based on Adam optimizer with an initial learning rate of 0.0001, which begins to decline linearly in the last 100 epochs. A batch size of 8 sample pairs is adopted due to the limitation on GPU memory. Data augmentation were applied during model training, including randomly clipping, rotation, and flipping. After training, all selected models were compared on the test set. The adversarial training process lasts for 10000 epochs, in which the batch size is set to 2. Both the generator and the discriminator employ an initial learning rate of 0.0001. All experiments are implemented in PyTorch environments and are conducted on the GeForce RTX 2080ti to accelerate model training

3.5 Accuracy Evaluation

Five indices are involved in the evaluation, including precision (Pre), recall (Rec), F1-score, intersection-over-union (IoU), and overall accuracy (OA). Given that TP, FP, TN and FN refer to true positives, false positives, true negatives, and false negatives, respectively, these indices can be defined as follows

$$Pre = \frac{TP}{TP+FP} \tag{8}$$

$$Rec = \frac{TP}{TP+FN} \tag{9}$$

$$F1 = \frac{2 precision \cdot recall}{precision + recall} \tag{10}$$

$$IoU = \frac{TP}{FP+TP+FN} \tag{11}$$

$$OA = \frac{TP+TN}{FP+TP+FN+TN} \tag{12}$$

During the pre-training process, the Pre, Rec, F1 and IoU are utilized to measure the model performance on UGSet, which are commonly used in semantic segmentation tasks. On the other and, the Pre, Rec, F1 and OA indices are employed to verify the accuracy of the generated UGS maps (UGS-1m).

4 Results

4.1 Accuracy evaluation on UGS-1m

An overview of the UGS-1m product is provided in Figure 9. Since there is no large-scale and fine-grained UGS ground truth for accuracy evaluation, five cities from different regions are selected to evaluate the reliability of the UGS results in the UGS-1m, including Changchun, Beijing, Wuhan, Guangzhou and Lhasa, as shown in Figure 10. Totally 17 sample tiles are collected from the five cities, among which Changchun, Beijing and Guangzhou each contributed four tiles. Due to the relatively small building area, 3 and 2 tiles were collected from Wuhan and Lhasa respectively. The UGS annotations of all tiles are obtained by expert interpretation. The accuracy evaluation is conducted according to the annotated reference map and the result in UGS-1m.

The evaluation results are summarized in Table 2, which are evaluated by OA, Pre, Rec and F1. It can be seen that in the five cities for verification, the average OA in all cities is 87.56%, while the OA of each city is higher than 85%. Among them,

Table 2. Quantitative results of accuracy evaluation on UGS-1m.

City	Number of tiles	OA(%)	Pre(%)	Rec(%)	F1(%)
Changchun	4	90.62	78.55	75.70	77.10
Beijing	4	85.86	78.72	79.74	79.23
Guangzhou	4	87.40	78.73	83.70	81.14
Wuhan	3	86.05	63.73	72.21	67.71
Lhasa	2	87.46	55.75	64.59	59.85
Average		87.56	73.33	76.61	74.86

the highest OA is 90.62% in Changchun, while the lowest OA also reaches 85.86% in Beijing, indicating that the UGS results in different cities is basically good. In terms of F1 score, Guangzhou has the highest F1 score of 81.14%, followed by Beijing and Changchun with the F1 of 79.23% and 77.23%, respectively. Though the F1 scores of Wuhan and Lhasa are relatively low, of 67.71% and 59.85%, respectively, the average F1 score of the final UGS results also reaches 74.86%. Moreover, the average

300 Recall of 76.61% also denotes a relatively low missed-detection rate of the UGS extraction results, which is significantly important in applications. In general, after quantitative validation in several different cities, the availability of UGS-1m is preliminarily demonstrated.

4.2 Qualitative analysis on UGS-1m

The qualitative analysis is carried out to further analyze the performance of UGS extraction as well as its relationship with

305 external factors, such as geographical location, UGS types, phenological phase, for etc. Therefore, visualization comparisons conducted in three cities, including Changchun, Wuhan and Guangzhou, are displayed in Figure 11-13.

From the overview image of Changchun and Guangzhou (Figure 11 and Figure 12), it can be seen that the extracted UGS results are in good agreement with the reference map, which is mainly reflected in the good restoration of UGS of various scales in each example image. The zoom-in area of each image further shows the details of UGS-1m for extracting different

310 kinds of UGS, including park, square, green buffer, as well as the attached green space. Specifically, the UGS-1m performs well in the extraction of green space attached to residential buildings, although they are complex and broken in morphology compared to other UGS types. Notably, although Changchun and Guangzhou are geographically far away, distributed in the northernmost and southernmost regions of China respectively, the UGS results in these two cities are both good. This shows that the performance of the proposed USG extraction framework is unlikely to be affected by the difference of geographical

315 location, which may attribute to the adversarial training strategy to model transferring.

The visualization result of Wuhan is further provided in Figure 13 for analysis. The UGS extraction results in Wuhan are mainly influenced by the shadow of buildings. On the one hand, the UGS features are sometimes blocked by building shadows, resulting in relatively poor extraction effect, such as the zoom-in area of Figure 13 - (b). On the other hand, the building shadows can easily be extracted as attached green space, according to Figure 13 - (c). This shows that the result of green space

320 extraction is related to the image taking angle. When the angle is larger, it is more likely to have building shadows in the image
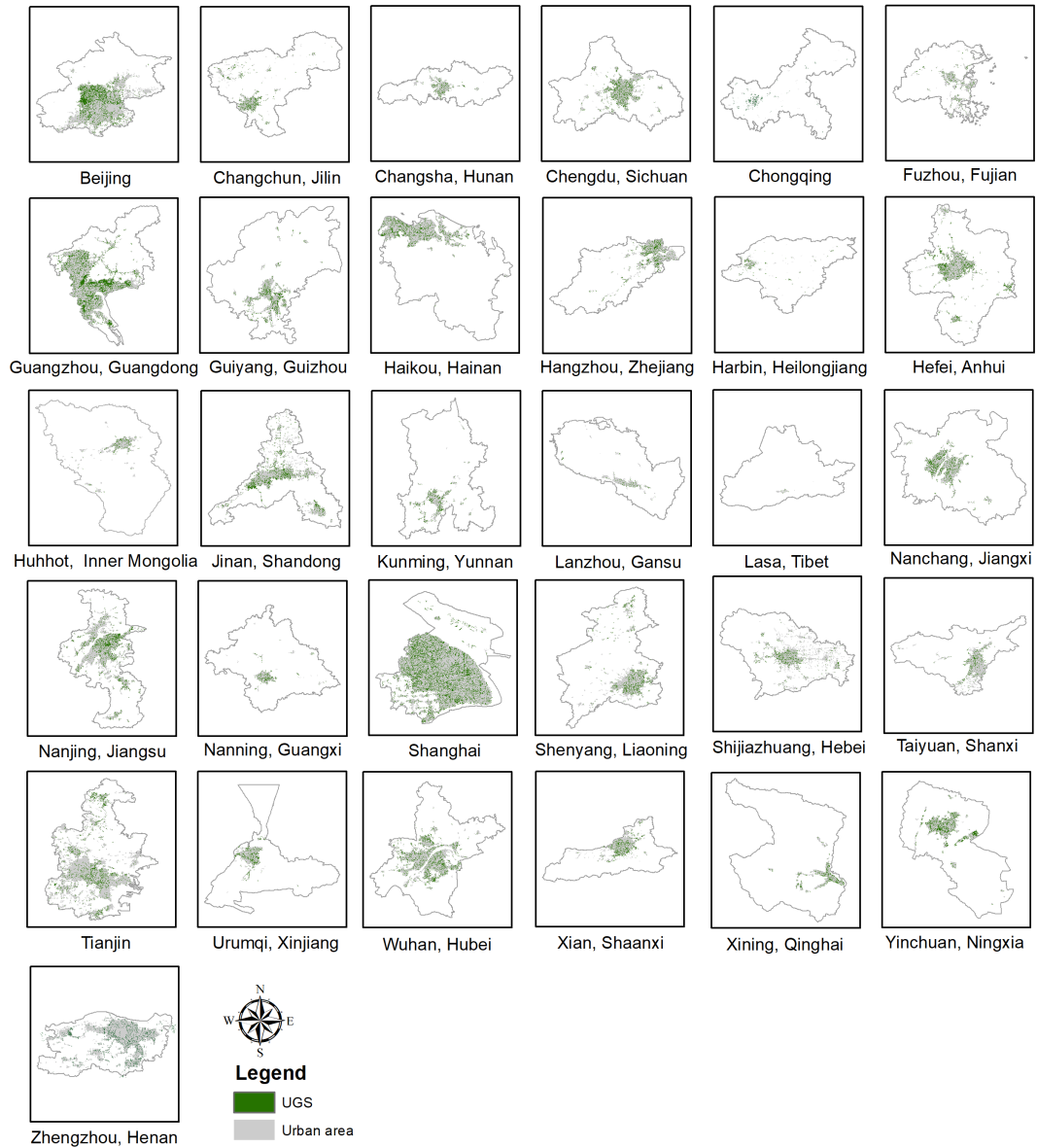
Figure 9. UGS results of the 34 31 major cities /areas in China (UGS-1m).

and thus affecting the subsequent UGS extraction, especially the green space that attached to buildings. In addition, the results are also affected by phenological phase, as shown in Figure 13 - (a). On the whole, it can be seen that the UGS with higher and denser vegetation canopy is easier to be identified accurately, and on the contrary, the lower and sparser UGS is more easily to be misclassified due to the similar appearance with other land types, such as the bare land.
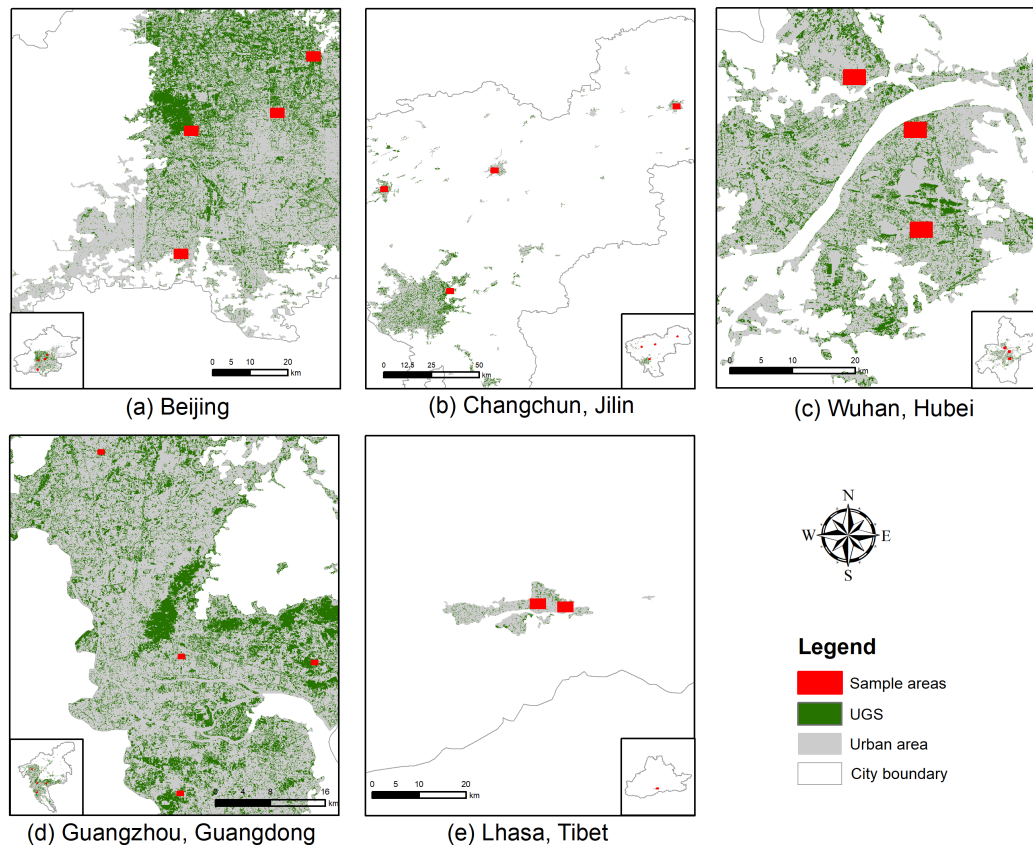
Figure 10. Sample areas for accuracy evaluation. (a) Beijing City; (b) Changchun City, Jilin Province; (c) Wuhan City, Hubei Province; (d) Guangzhou City, Guangdong Rovince; (d) Lhasa City, Tibet Autonomous Region.

4.3 Comparison with existing products

We compare the UGS-1m results with existing global land use products to verify the reliability of the results, including GlobeLand30 (Chen and Chen, 2018), GLC_FCS30 (Zhang et al., 2021) and Esri 2020 LC (© 2021 Esri). Due to different classification systems, these products need to be reclassified in two categories first. Specifically, forests, grasslands and shrublands are reclassified as UGS, while the other categories are reclassified as non-UGS. Examples from 6 different cities of different latitudes, including Changchun, Urumqi, and Beijing, Chengdu, Wuhan and Guangzhou, are collected to give more comprehensive demonstrations on our UGS results. The visualization comparison among UGS-1m, GlobeLand30, GLC_FCS30 and Esri 2020 LC is shown in Figure 14. Apparently, the three comparative products contain most large-scale UGS, among which the GlobeLand30 performs best with most complete UGS prediction. However, many detailed UGS features are still missed due to the limitation on spatial resolution of source image. On the other hand, the UGS-1m provides UGS with relatively
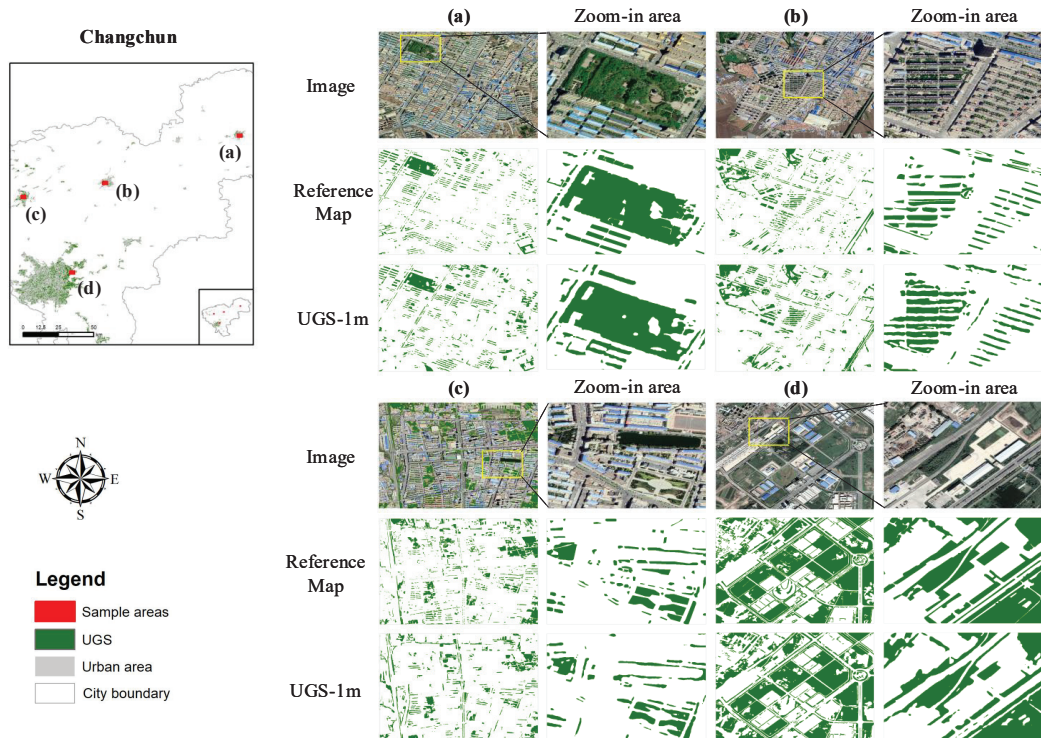
Figure 11. Qualitative analysis on UGS-1m: case study in Changchun City. (a)-(d) are four example areas collected from Changchun (Images © Google Earth 2020).

large scale, as well as detailed UGS information such as attached green space. The results and comparisons fully demonstrate the effectiveness and potential of the proposed deep learning framework for large-scale and fine-grained UGS mapping.

4.4   UGS Statistics and analysis based on UGS-1m

While the previous evaluation and comparisons have proved the advantages and validity of the UGS-1m, this section would like to explore the potential utility of the UGS-1m product. As mentioned above in the Introduction section, green space equality is one of the keys for the Sustainable Development, which requires fine-grained distributions of UGS as basic data. At this point, compared with the traditional statistical yearbook data, our UGS-1m product can provide a relatively objective and more detailed information about the distribution of green space. Therefore, statistics is conducted on the UGS-1m data to obtain information of the UGS area and the UGS rate in the GUB area, which are summarized in Table Table 3.

As shown in Table Table 3, the area of green space in different cities varies greatly. For example, its obtained that the UGS area of Beijing is the largest among all the 31 cities studied, reaching 1,021.55 square kilometers, while that of Lhasa is the smallest with only 11.41 square kilometers. The statistical area information indicates that the UGS-1m can provide a quick and intuitive comparison of the stock of urban green space in different cities. However, a small UGS area does not always mean
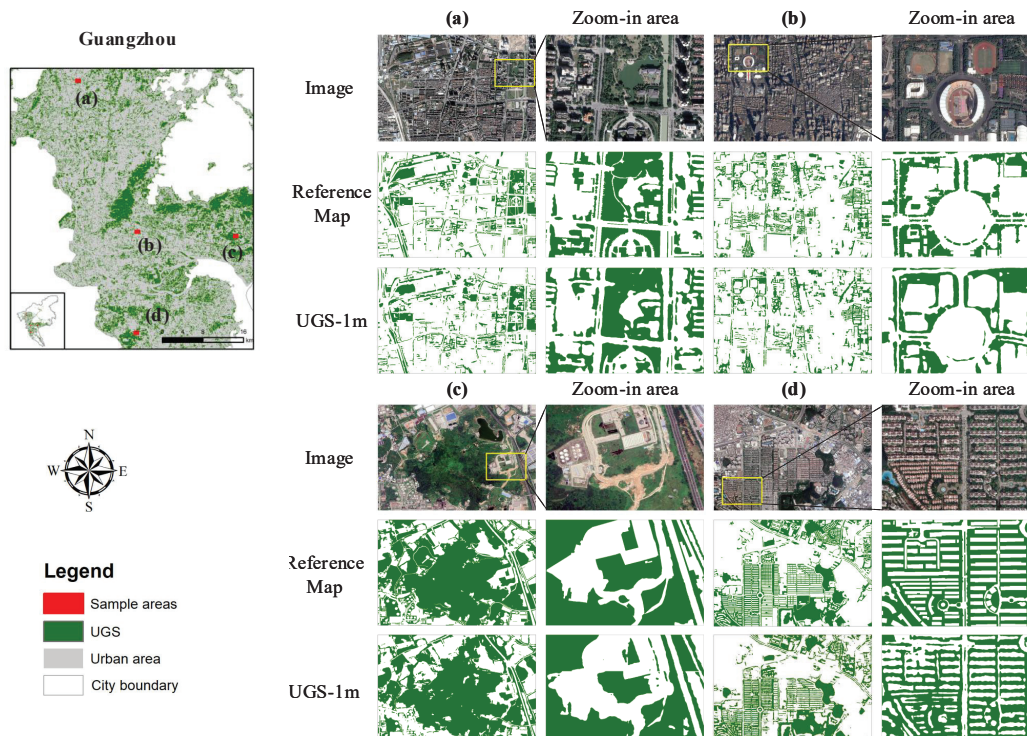
Figure 12. Qualitative analysis on UGS-1m: case study in Guangzhou City. (a)-(d) are four example areas collected from Guangzhou (Images © Google Earth 2020).

the lack of green space due to the restrictions on the city area. Therefore, the UGS rate in the GUB area is further calculated to measure the deficiency and inequality of green space in different cities. At this time, it can be seen that Yinchuan has the highest UGS rate, accounting for 25.35%, while Beijing, which has the largest UGS area, has a slightly lower UGS rate of 20.74%. Besides, the UGS rate of 9.27% in Lhasa, which has the least UGS area, is also slightly better than that of Lanzhou, which has the lowest UGS rate of 8.64%. The results and comparisons further show that the shortage and imbalance of green space cannot be reflected only from the perspective of the stock of green space, and more information and data are often needed for analysis.

The above statistical analysis only shows the most simple and intuitive applicability of UGS-1m as a large-scale and refined green space product, but it is far more than that. Since the high-resolution UGS-1m can provide the detailed distribution of green space, it brings possibility to research in fine-grained scenarios. When considering different datasets or materials, more comprehensive information of UGS can be obtained. For example, by combining high-resolution population (e.g. Worldpop data) with UGS-1m, the availability of residents to green space can be measured, that is, green space equity. Or, combined with the distribution of slums and formal housing space, their differences in green landscape pattern can be studied. We also hope to explore these works in the future.

Table 3. Statistical results on UGS-1m of UGS area and rate for the 31 major cities in China.

Id	City	Province	GUB area (Sq.Km)	UGS area (Sq.Km)	UGS Rate in GUB (%)
0	Beijing	/	4925.08	1021.55	20.74
1	Changchun	Jilin	1405.23	331.56	23.59
2	Changsha	Hunan	887.87	162.46	18.30
3	Chengdu	Sichuan	1813.62	336.67	18.56
4	Chongqing	/	1956.56	449.11	22.95
5	Fuzhou	Fujian	1140.41	142.85	12.53
6	Guangzhou	Guangdong	2552.02	561.46	22.00
7	Guiyang	Guizhou	605.05	107.31	17.74
8	Haikou	Hainan	291.81	43.10	14.77
9	Hangzhou	Zhejiang	2217.51	399.74	18.03
10	Harbin	Heilongjiang	1399.12	290.58	20.77
11	Hefei	Anhui	1288.46	281.95	21.88
12	Hohhot	Inner Mongolia	546.26	83.58	15.3
13	Jinan	Shandong	2087.83	424.37	20.33
14	Kunming	Yunnan	1082.19	183.41	16.95
15	Lanzhou	Gansu	444.97	38.46	8.64
16	Lasa	Tibet	123.09	11.41	9.27
17	Nanchang	Jiangxi	637.85	128.35	20.12
18	Nanjing	Jiangsu	1651.83	289.77	17.54
19	Nanning	Guangxi	680.96	116.21	17.07
20	Shanghai	/	4245.44	852.07	20.07
21	Shenyang	Liaoning	1455.37	311.04	21.37
22	Shijiazhuang	Hubei	1844.85	262.28	14.22
23	Taiyuan	Shanxi	817.78	106.38	13.01
24	Tianjin	/	3457.96	496.77	14.37
25	Urumqi	Xinjiang	985.78	199.24	20.21
26	Wuhan	Hubei	1665.88	290.44	17.43
27	Xian	Shaanxi	1330.58	264.33	19.87
28	Xining	Qinghai	262.09	52.89	20.18
29	Yinchuan	Ningxia	612.71	155.35	25.35
30	Zhengzhou	Henan	2311.41	302.04	13.07

[*] The "/" in Province column denotes a municipality city.
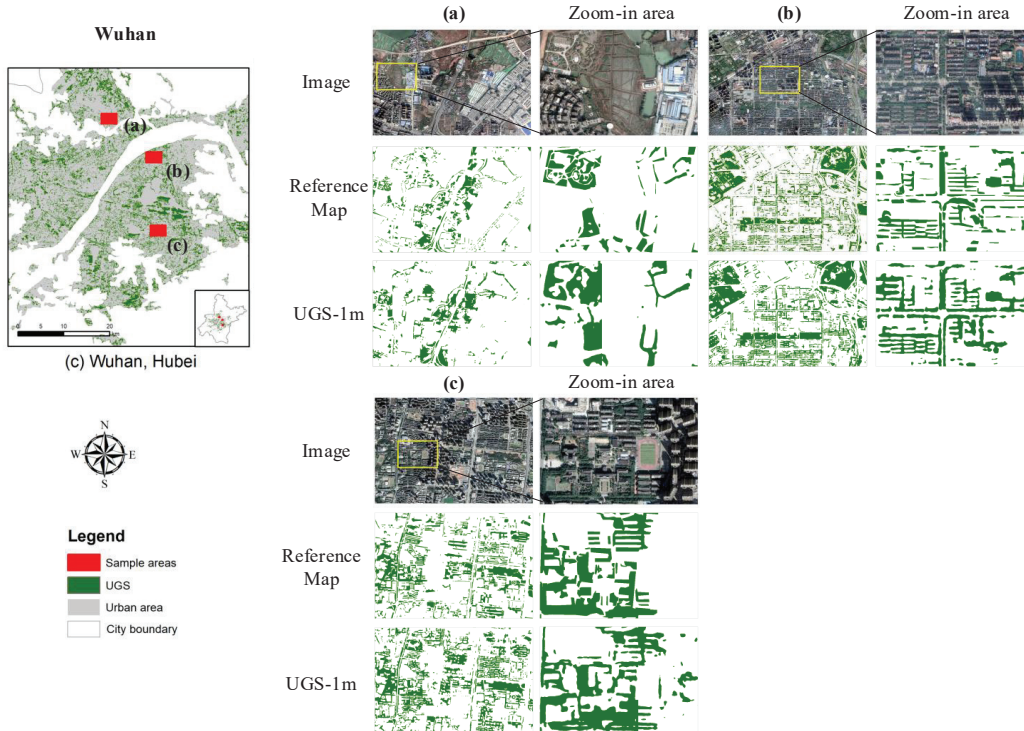
Figure 13. Qualitative analysis on UGS-1m: case study in Wuhan City. (a)-(c) are three example areas collected from Wuhan (Images © Google Earth 2020).

5 Discussions

5.1 Comparative experiments at pre-training stage

As we have mentioned above, before the start of adversarial training stage, the generator will be initialized by a pre-trained UGSNet on UGSet. Therefore, in order to fully verify the advancement of UGSNet and its qualification to initialize the generator, this section introduces several state-of-the-art (SOTA) deep learning models as candidate generators for comparison. Noted that the comparative experiment is completely conducted on UGSet, and no discriminator is introduced. After all the models have been fully trained on training set of the UGSet, the best-trained model of each model will be evaluated on the testing set of the UGSet. The comparative results are provided in Table 4.

As Table 4 shows, the proposed UGSNet outperforms all SOTA baselines with the highest F1 and IoU of 77.30% and 62.99%, respectively. The second-ranked PSPNet obtains an IoU of 60.96%, which is 2.03% lower than that of UGSNet. The ablation study indicates that the integration of the ECA modules and point head can improve the Base model by 0.17% and 0.69% on IoU, respectively, which proves their effectiveness on UGS extraction. The IoU of UGSNet is 1.22% higher than that
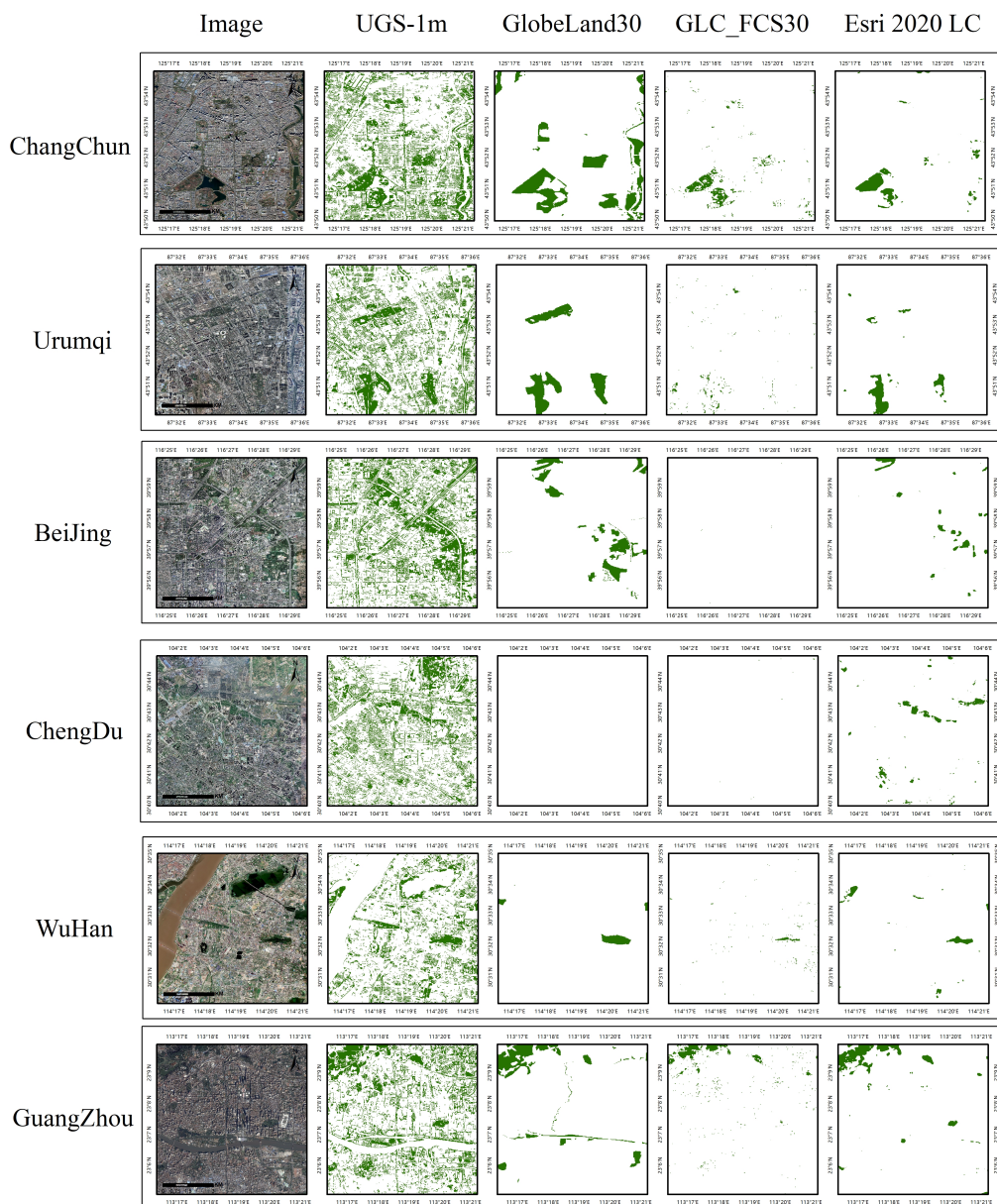
Figure 14. Visualization comparisons between UGS-1m, GlobeLand30 (Chen and Chen, 2018), GLC_FCS30 (Zhang et al., 2021) and Esri 2020 LC (© 2021 Esri) (Images © Google Earth 2020).

of the Base model, indicating that the combination of ECA modules and point head has a greater gain effect. The quantitative results demonstrate the validity of UGSNet.

375

Table 4. Performance of different semantic segmentation methods on UGSet.

Method	Pre(%)	Rec(%)	F1(%)	IoU(%)
SegNet	71.70	77.34	74.42	59.26
UNet	75.57	74.92	75.25	60.31
UperNet	74.81	76.11	75.45	60.58
BiSeNet	75.13	76.26	75.69	60.89
PSPNet	76.57	74.94	75.74	60.96
Base	76.52	76.22	76.37	61.77
Base+ECA	**76.87**	76.13	76.49	61.94
Base+PointHead	74.99	78.89	76.89	62.46
UGSNet	75.40	**79.29**	**77.30**	**62.99**

Figure 15 further demonstrates the performance of different methods on different kinds of UGS. It can be seen that after fully training on UGSet dataset, each model can identify the approximate region of various green spaces, including SegNet, which has shown poor performance in quantitative comparisons. Therefore, the superiority of green space identification results is mainly reflected in two aspects. One aspect is the ability to extract UGS of great inter-class similarity. As shown in the first row of Figure 15, the UGSNet can accurately identify the yellow box area, in which the green space of park has confused most comparative methods. Another aspect is the capability to grasp fine-grained edges, especially for small-scale UGS, such as the attached UGS in the last row of Figure 15.

5.2 Ablation study on the discriminator

As we have mentioned above, the proposed framework is composed of a generator and a discriminator, which adopts the adversarial training to help model transfer learning. In order to test the effectiveness of the proposed framework, this section further conducted ablation experiments on the with and without the discriminator, which respectively correspond to:

(1)Our framework ($G+D$): contains a generator and a discriminator, in which the generator is initialized by the UGSNet pre-trained on UGSet, and the discriminator is employed at the adversarial training stage to overcome domain shifts and obtain a refined UGSNet for each target city/area, before generating the UGS map for it;

(2) UGSNet (only D): no discriminator is involved, simply applying the pre-trained UGSNet to each target city/area and generate their UGS maps, regardless of the domain shifts between the UGSet and images from different target cities/areas.

The result of "Our framework ($G+D$)" comes from quantitative results of UGS-1m in Sect. 4. In order to test the effect of "UGSNet (only G)", the pre-trained UGSNet is applied to the same sample areas for accuracy evaluation. The final ablation results are shown in Table 5. It can be seen from the results that when the discriminator is not used, the OA of almost all cities decreases to a certain extent. Generally speaking, the average OA decreases from 87.56% to 85.73%. The F1 score shows a sharp decline, with the average F1 score dropping from 74.86% to 60.18%. Specifically, the decline of F1 score in Guangzhou and Beijing is relatively small, which indicates that the difference between the images of these two cities and the UGSet images

| (a) | (b) | (c) | (d) | (e) | (f) | (g) | (h) | (i) | (j) | (k) |
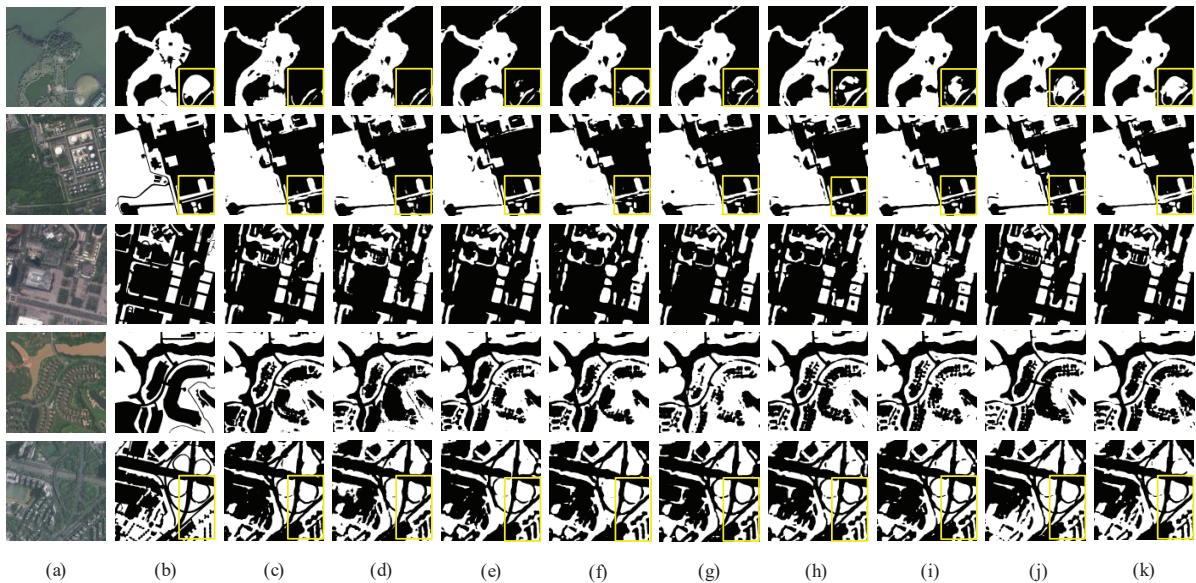
Figure 15. Visualization comparisons of different methods on UGSet (Images were retrieved from ~~GF-2~~ Gaofen-2 2019). (a) Image; (b) Label; (c) SegNet; (d) UNet; (e) UperNet; (f) BiSeNet; (g) PSPNet; (h) Base; (i) Base+ECA; (j) Base+Point Head; (k) UGSNet.

Table 5. Ablation study on the discriminator(D).

City	Our framework ($G+D$)		UGSNet (only G)	
	OA(%)	F1(%)	OA(%)	F1(%)
Changchun	90.62	77.10	86.34	54.57
Beijing	85.86	79.23	84.82	75.59
Guangzhou	87.4	81.14	85.33	75.49
Wuhan	86.05	67.71	86.56	62.47
Lhasa	87.46	59.85	85.86	6.51
Average	87.56	74.86	85.73	60.18

is not that significant. Therefore, the pre-trained model can capture some UGS. It is worth noting that the use of discriminator can significantly improve the results in Changchun, according to the great growth of F1 score of 22.53%. Moreover, the results in Lhasa, only have an F1 score of 6.51% without D, which can reach 59.85% when using D. The ablation experiment fully proves the effectiveness and potential of the proposed framework for large-scale green space mapping.

5.3 ~~Comparison with existing products~~

~~We compare the UGS-1m results with existing global land use products to verify the reliability of the results, including GlobeLand30 (Chen and Chen, 2018), GLC_FCS30 (Zhang et al., 2021) and Esri 2020 LC (© 2021 Esri). Due to different~~
405 ~~classification systems, these products need to be reclassified in two categories first. Specifically, forests, grasslands and shrublands are reclassified as UGS, while the other categories are reclassified as non-UGS. Examples from 6 different cities of different latitudes, including Changchun, Urumqi, and Beijing, Chengdu, Wuhan and Guangzhou, are collected to give more comprehensive demonstrations on our UGS results. The visualization comparison among UGS-1m, GlobeLand30, GLC_FCS30 and Esri 2020 LC is shown in Figure 14. Apparently, the three comparative products contain most large-scale UGS, among~~
410 ~~which the GlobeLand30 performs best with most complete UGS prediction. However, many detailed UGS features are still missed due to the limitation on spatial resolution of source image. On the other hand, the UGS-1m provides UGS with relatively large scale, as well as detailed UGS information such as attached green space. The results and comparisons fully demonstrate the effectiveness and potential of the proposed deep learning framework for large-scale and fine-grained UGS mapping. Visualization comparisons between UGS-1m, GlobeLand30 (Chen and Chen, 2018), GLC_FCS30 (Zhang et al., 2021) and~~
415 ~~Esri 2020 LC (© 2021 Esri) (Images © Google Earth 2020).~~

5.3 Limitations and future work

At present, the availability of high-resolution images is still severely limited by factors such as temporal resolution, image distortion and cloud occlusion. Therefore, the Google Earth images used to produce UGS-1m are very difficult to collect at one time, so it is difficult to ensure the unity of phenology. In the proposed deep learning framework, we introduce domain
420 adaptation to deal with this problem to some extent. Comparison results had shown the effectiveness of UGS-1m, as well as the feasibility and potential of the proposed deep learning framework for large-scale, high-resolution mapping. Future works will be dedicated to extract UGS information based on data with higher temporal resolution, such as SAR images and unmanned aerial vehicle (UAV) images. Future works will be dedicated to extract UGS information based on data with higher temporal resolution, such as SAR images and unmanned aerial vehicle (UAV) images.

425 Besides, even though the UGSet have proved to be practicable for UGS mapping, we still have to point out that there may be a small number of missing labels in the dataset, especially for attached green spaces. As analyzed above, the extraction of attached green space can be more easily to be affected by external factors, like image taking angle, and the process of annotation is the same. Fortunately, despite the possible deficiencies, the DL model can still learn from a large number of accurate annotations, and capture the characteristics of different types of green spaces due to the strong generalization ability.
430 We still hope that in the following work, more attempts can be made on the problems of labeling and identification of hard UGS types.

6 Code and data availability

The UGS-1m product can be downloaded at https://doi.org/10.5281/zenodo.6155516 (Shi et al., 2022). They are named by name of the ~~34 cities/areas~~31 cities.

The Dataset and Code for the deep learning framework will be available at https://liumency.github.io/UGS-1m/.

7 Conclusions

In this paper, we propose a novel deep learning (DL) framework for large-scale UGS mapping, and generate the fine-grained UGS maps for ~~34 major cities /area~~ 31 major cities in China (UGS-1m). The accuracy evaluation on the UGS-1m products indicates the reliability and applicability. Comparative experiments conducted on UGSet among several SOTA semantic segmentation networks show that UGSNet can achieve the best performance on UGS extraction. The ablation study on UGSNet also demonstrates the effectiveness of the ECA module and point head. Comparisons between UGS-1m and existing land use products have proved the validity of the proposed DL framework for large-scale and fine-grained UGS mapping. The achievements provided in this paper can support the scientific community for UGS understanding and characterization, and pave the way for the development of robust and efficient methods able to tackle the current limits and needs of UGS analysis in technical literature.

Author contributions. Qian Shi: Conceptualization, Resources, Investigation, Funding acquisition and Writing – review & editing; Mengxi Liu: Data curation, Methodology, Validation, Formal analysis, Visualization and Writing – original draft preparation; Andrea Marinoni: Writing – review & editing; Xiaoping Liu: Writing – review & editing.

Competing interests. The authors declare that they have no conflict of interest.

Acknowledgements. This study is supported in part by the National Natural Science Foundation of China under Grant 61976234, in part by Centre for Integrated Remote Sensing and Forecasting for Arctic Operations (CIRFA) and the Research Council of Norway (RCN Grant no. 237906), and the Visual Intelligence Centre for Research-based Innovation funded by the Research Council of Norway (RCN Grant no. 309439).

References

455 Badrinarayanan, V., Kendall, A., and Cipolla, R.: Segnet: A deep convolutional encoder-decoder architecture for image segmentation, IEEE transactions on pattern analysis and machine intelligence, 39, 2481–2495, https://doi.org/https://doi.org/10.1109/TPAMI.2016.2644615, 2017.

    Cao, Y. and Huang, X.: A deep learning method for building height estimation using high-resolution multi-view imagery over urban areas: A case study of 42 Chinese cities, Remote Sensing of Environment, 264, 112 590, 2021.

460 Chen, B., Tu, Y., Wu, S., Song, Y., Jin, Y., Webster, C., Xu, B., and Gong, P.: Beyond green environments: multi-scale difference in human exposure to greenspace in China, Environment International, 166, 107 348, 2022a.

    Chen, B., Wu, S., Song, Y., Webster, C., Xu, B., and Gong, P.: Contrasting inequality in human exposure to greenspace between cities of Global North and Global South, Nature Communications, 13, 1–9, 2022b.

    Chen, J. and Chen, J.: GlobeLand30: Operational global land cover mapping and big-data analysis, Science China. Earth Sciences, 61,
465 1533–1534, 2018.

    Chen, L.-C., Zhu, Y., Papandreou, G., Schroff, F., and Adam, H.: Encoder-decoder with atrous separable convolution for semantic image segmentation, 2018a.

    Chen, W., Huang, H., Dong, J., Zhang, Y., Tian, Y., and Yang, Z.: Social functional mapping of urban green space using remote sensing and social sensing data, ISPRS Journal of Photogrammetry and Remote Sensing, 146, 436–452, 2018b.

470 Daudt, R. C., Saux, B. L., and Boulch, A.: Fully Convolutional Siamese Networks for Change Detection, IEEE, 2018.

    De Ridder, K., Adamec, V., Ba N Uelos, A., Bruse, M., B U Rger, M., Damsgaard, O., Dufek, J., Hirsch, J., Lefebre, F., P E Rez-Lacorzana, J. M., and Others: An integrated methodology to assess the benefits of urban green space, Science of the total environment, 334, 489–497, https://doi.org/https://doi.org/10.1016/j.scitotenv.2004.04.054, 2004.

    Deng, L. and Yu, D.: Deep Learning: Methods and Applications, Foundations & Trends in Signal Processing, 7, 197–387, 2014.

475 Devlin, J., Chang, M., Lee, K., and Toutanova, K.: BERT: Pre-training of Deep Bidirectional Transformers for Language Understanding, CoRR, abs/1810.04805, http://arxiv.org/abs/1810.04805, 2018.

    Everingham, M., Eslami, S. A., Van Gool, L., Williams, C. K., Winn, J., and Zisserman, A.: The pascal visual object classes challenge: A retrospective, International journal of computer vision, 111, 98–136, https://doi.org/https://doi.org/10.1007/s11263-014-0733-5, 2015.

    Fuller, R. A., Irvine, K. N., Devine-Wright, P., Warren, P. H., and Gaston, K. J.: Psychological benefits of greenspace increase with biodiver-
480 sity, Biology letters, 3, 390–394, https://doi.org/https://doi.org/10.1098/rsbl.2007.0149, 2007.

    General Office of the State Council, PRC: Guidelines on scientific greening, [Online], https://www.mee.gov.cn/zcwj/gwywj/202106/t20210603_836084.shtml (accessed June 3, 2021), 2021.

    Glorot, X., Bordes, A., and Bengio, Y.: Deep Sparse Rectifier Neural Networks, Journal of Machine Learning Research, 15, 315–323, 2011.

    Gong, P., Wang, J., Yu, L., Zhao, Y., Zhao, Y., Liang, L., Niu, Z., Huang, X., Fu, H., Liu, S., Li, C., Li, X., Fu, W., Liu, C., Xu, Y., Wang, X.,
485 Cheng, Q., Hu, L., Yao, W., Zhang, H., Zhu, P., Zhao, Z., Zhang, H., Zheng, Y., Ji, L., Zhang, Y., Chen, H., Yan, A., Guo, J., Yu, L., Wang, L., Liu, X., Shi, T., Zhu, M., Chen, Y., Yang, G., Tang, P., Xu, B., Giri, C., Clinton, N., Zhu, Z., Chen, J., and Chen, J.: Finer resolution observation and monitoring of global land cover: first mapping results with Landsat TM and ETM+ data, International journal of Remote Sensing, 34, 2607–2654, https://doi.org/10.1080/01431161.2012.748992, 2013.

Gong, P., Li, X., Wang, J., Bai, Y., Chen, B., Hu, T., Liu, X., Xu, B., Yang, J., Zhang, W., and Zhou, Y.: Annual
490   maps of global artificial impervious area (GAIA) between 1985 and 2018, Remote Sensing of Environment, 236, 111 510, https://doi.org/https://doi.org/10.1016/j.rse.2019.111510, 2020.

Helber, P., Bischke, B., Dengel, A., and Borth, D.: Eurosat: A novel dataset and deep learning benchmark for land use and land cover classification, IEEE journal of Selected Topics in Applied Earth Observations and Remote Sensing, 2019.

Hou, Q., Zhou, D., and Feng, J.: Coordinate Attention for Efficient Mobile Network Design, 2021.

495 Huang, C., Yang, J., Lu, H., Huang, H., and Yu, L.: Green spaces as an indicator of urban health: evaluating its changes in 28 mega-cities, Remote Sensing, 9, 1266, https://doi.org/https://doi.org/10.3390/rs9121266, 2017.

Huang, C., Yang, J., and Jiang, P.: Assessing impacts of urban form on landscape structure of urban green spaces in China using Landsat images based on Google Earth Engine, Remote Sensing, 10, 1569, https://doi.org/https://doi.org/10.3390/rs10101569, 2018.

Ioffe, S. and Szegedy, C.: Batch Normalization: Accelerating Deep Network Training by Reducing Internal Covariate Shift, CoRR,
500   abs/1502.03167, http://arxiv.org/abs/1502.03167, 2015.

Jun, C., Ban, Y., and Li, S.: China: Open access to Earth land-cover map, Nature, 514, 434–434, https://doi.org/https://doi.org/10.1038/514434c, 2014.

Kirillov, A., Wu, Y., He, K., and Girshick, R.: PointRend: Image Segmentation As Rendering, in: 2020 IEEE/CVF Conference on Computer Vision and Pattern Recognition (CVPR), pp. 9796–9805, https://doi.org/10.1109/CVPR42600.2020.00982, 2020.

505 Kong, F., Yin, H., James, P., Hutyra, L. R., and He, H. S.: Effects of spatial pattern of greenspace on urban cooling in a large metropolitan area of eastern China, Landscape and Urban Planning, 128, 35–47, https://doi.org/https://doi.org/10.1016/j.landurbplan.2014.04.018, 2014.

Krizhevsky, A., Sutskever, I., and Hinton, G. E.: Imagenet classification with deep convolutional neural networks, Advances in neural information processing systems, 25, 1097–1105, 2012.

Kuang, W. and Dou, Y.: Investigating the patterns and dynamics of urban green space in China's 70 major cities using satellite remote
510   sensing, Remote Sensing, 12, 1929, https://doi.org/https://doi.org/10.3390/rs12121929, 2020.

Li, X., Gong, P., Zhou, Y., Wang, J., Bai, Y., Chen, B., Hu, T., Xiao, Y., Xu, B., Yang, J., Liu, X., Cai, W., Huang, H., Wu, T., Wang, X., Lin, P., Li, X., Chen, J., He, C., Li, X., Yu, L., Clinton, N., and Zhu, Z.: Mapping global urban boundaries from the global artificial impervious area (GAIA) data, Environmental Research Letters, 15, 094 044, https://doi.org/10.1088/1748-9326/ab9be3, 2020.

Litjens, G., Kooi, T., Bejnordi, B. E., Setio, A. A. A., Ciompi, F., Ghafoorian, M., van der Laak, J. A., van Ginneken,
515   B., and Sánchez, C. I.: A survey on deep learning in medical image analysis, Medical Image Analysis, 42, 60–88, https://doi.org/https://doi.org/10.1016/j.media.2017.07.005, 2017.

Liu, M., Shi, Q., Marinoni, A., He, D., and Zhang, L.: Super-resolution-based Change Detection Network with Stacked Attention Module for Images with Different Resolutions, 2021.

Liu, P., Liu, X., Liu, M., Shi, Q., Yang, J., Xu, X., and Zhang, Y.: Building Footprint Extraction from High-Resolution Images via Spatial
520   Residual Inception Convolutional Neural Network, Remote Sensing, 11, 2019a.

Liu, W., Yue, A., Shi, W., Ji, J., and Deng, R.: An Automatic Extraction Architecture of Urban Green Space Based on DeepLabv3plus Semantic Segmentation Model, 2019b.

Mathieu, R., Aryal, J., and Chong, A. K.: Object-based classification of Ikonos imagery for mapping large-scale vegetation communities in urban areas, Sensors, 7, 2860–2880, https://doi.org/https://doi.org/10.3390/s7112860, 2007.

525 Ministry of Housing and Urban-Rural Development, PRC: Urban Green Space Planning Standard (GB/T51346-2019), https://www.mohurd. gov.cn/gongkai/fdzdgknr/tzgg/201910/20191012_242194.html (accessed April 9, 2019), 2019.

Ronneberger, O., Fischer, P., and Brox, T.: U-net: Convolutional networks for biomedical image segmentation, pp. 234–241, 2015.

Shi, Q., Liu, M., Li, S., Liu, X., Wang, F., and Zhang, L.: A deeply supervised attention metric-based network and an open aerial image dataset for remote sensing change detection, IEEE Transactions on Geoscience and Remote Sensing, https://doi.org/https://doi.org/10.1109/TGRS.2021.3085870, 2021.

Shi, Q., Liu, M., and Marinoni, A.: UGS-1m: Fine-grained urban green space mapping of 34 major cities in China based on the deep learning framework [Data set], Zenodo, https://doi.org/10.5281/zenodo.6155516, 2022.

Sun, J., Wang, X., Chen, A., Ma, Y., Cui, M., and Piao, S.: NDVI indicated characteristics of vegetation cover change in China's metropolises over the last three decades, Environmental monitoring and assessment, 179, 1–14, https://doi.org/https://doi.org/10.1007/s10661-010-1715-x, 2011.

Tsai, Y.-H., Hung, W.-C., Schulter, S., Sohn, K., Yang, M.-H., and Chandraker, M.: Learning to Adapt Structured Output Space for Semantic Segmentation, in: IEEE Conference on Computer Vision and Pattern Recognition (CVPR), 2018.

Vaswani, A., Shazeer, N., Parmar, N., Uszkoreit, J., Jones, L., Gomez, A. N., Kaiser, Ł., and Polosukhin, I.: Attention is all you need, Advances in neural information processing systems, 30, 2017.

Woo, S., Park, J., Lee, J.-Y., and Kweon, I. S.: Cbam: Convolutional block attention module, in: Proceedings of the European conference on computer vision (ECCV), pp. 3–19, 2018.

Wu, F., Wang, C., Zhang, H., Li, J., Li, L., Chen, W., and Zhang, B.: Built-up area mapping in China from GF-3 SAR imagery based on the framework of deep learning, Remote Sensing of Environment, 262, 112 515, https://doi.org/https://doi.org/10.1016/j.rse.2021.112515, 2021.

Xu, Z., Zhou, Y., Wang, S., Wang, L., Li, F., Wang, S., and Wang, Z.: A novel intelligent classification method for urban green space based on high-resolution remote sensing images, Remote Sensing, 12, 3845, https://doi.org/https://doi.org/10.3390/rs12223845, 2020.

Yang, J., Huang, C., Zhang, Z., and Wang, L.: The temporal trend of urban green coverage in major Chinese cities between 1990 and 2010, Urban Forestry & Urban Greening, 13, 19–27, https://doi.org/https://doi.org/10.1016/j.ufug.2013.10.002, 2014.

Zhang, B., Li, N., Wang, S., and Others: Effect of urban green space changes on the role of rainwater runoff reduction in Beijing, China, Landscape and Urban Planning, 140, 8–16, https://doi.org/https://doi.org/10.1016/j.landurbplan.2015.03.014, 2015.

Zhang, Q., Yang, L. T., Chen, Z., and Li, P.: A survey on deep learning for big data, Information Fusion, 42, 146–157, 2018.

Zhang, X., Liu, L., Chen, X., Gao, Y., Xie, S., and Mi, J.: GLC_FCS30: Global land-cover product with fine classification system at 30m using time-series Landsat imagery, Earth System Science Data, 13, 2753–2776, https://doi.org/10.5194/essd-13-2753-2021, 2021.

Zhao, J., Ouyang, Z., Zheng, H., Zhou, W., Wang, X., Xu, W., and Ni, Y.: Plant species composition in green spaces within the built-up areas of Beijing, China, Plant ecology, 209, 189–204, https://doi.org/https://doi.org/10.1007/s11258-009-9675-3, 2010.

Zhou, W., Wang, J., Qian, Y., Pickett, S. T., Li, W., and Han, L.: The rapid but "invisible" changes in urban greenspace: A comparative study of nine Chinese cities, Science of the Total Environment, 627, 1572–1584, https://doi.org/https://doi.org/10.1016/j.scitotenv.2018.01.335, 2018.

Zhou, X. and Wang, Y.-C.: Spatial-temporal dynamics of urban green space in response to rapid urbanization and greening policies, Landscape and urban planning, 100, 268–277, https://doi.org/https://doi.org/10.1016/j.landurbplan.2010.12.013, 2011.